UPGRADING DESIGN OF A MULTI-TW FEMTOSECOND LASER

V. ALEKSANDROV[1], G. BLEOTU[1,2,3], L. CARATAS[1], R. DABU[1]*, I. DANCUS[1], R. FABBRI[1], V. IANCU[1,2], B. ISPAS[1,2], M. KISS[1], A. LACHAPELLE[1], A. LAZAR[1], M. MASRURI[1], D. MATEI[1], M. MERISANU[1], A. NAZIRU[1,2], D. NISTOR[1], R. SECAREANU[1], M. TALPOSI[1,2], A. TOADER[1], A. TOMA[1], D. URSESCU[1].

[1]ELI-NP, "Horia Hulubei" National Institute for Nuclear Physics and Engineering, 30 Reactorului Street, RO-077126 Bucharest-Magurele, Romania
[2]University of Bucharest, Faculty of Physics, 077125 Bucharest-Magurele, Romania
[3]LULI, École Polytechnique, Route de Saclay, 91120, Palaiseau, France
**Corresponding author, e-mail: razvan.dabu@eli-np.ro*

Received June 9, 2020

Abstract. The configuration of a commercial TW-class femtosecond laser amplifier and measurement techniques used for laser pulse characterization are described. Designed laser modules and new laser system layout for upgrading this sub-TW femtosecond laser system to a multi-TW laser system are presented. A four-pass Ti:sapphire amplifier was designed to amplify the chirped pulses from 15 mJ up to 220 mJ energy. A vacuum compressor, with two-diffraction gratings, was designed for amplified pulses temporal compression. Considering 30 nm bandwidth input pulses with ideal Fourier transform limit (FTL) duration of 31.4 fs, 1.05 times FTL pulses can be obtained by the compensation of the chirped pulse amplifier phase dispersion in the compressor. Some experiments based on the upgraded multi-TW Ti:sapphire laser are proposed, such as spectral broadening for post-compression, laser induced damage threshold measurements using femtosecond pulses, and coherent combination of ultrashort pulses.

Key words: femtosecond oscillator, Ti:sapphire laser, chirped pulse amplification.

1. INTRODUCTION

The chirped pulse amplification (CPA) technique [1] has been used to make significant advances in the development of laser systems producing high-peak-power laser pulses. A remarkable progress has been achieved with femtosecond CPA

Ti:sapphire laser systems in the last 30 years. Beginning with hundred-GW to TW class CPA lasers in the early ‘90 years [2], passing through 100 TW [3,4] and 1 PW [5,6] Ti:sapphire laser systems, recently multi-PW peak power has been reported [7,8].

Such ultra-high-power laser systems are used in fundamental research areas, such as high field physics and the generation of ultra-short energetic electrons and ions [9,10]. Extreme-Light Infrastructure - Nuclear Physics (ELI-NP) laser facility, devoted to high-field laser research in nuclear physics, demonstrated the capability of 10 PW peak power in a two-arm laser system configuration [11]. The operation of such a complex laser facility requires high-level specialists in the field of high power laser systems physics and engineering.

A TW-class femtosecond laser amplifier has been acquired from the Avesta Company as an unassembled laser kit. We have installed and tuned this laser kit in the Optics Laboratory of the Laser Systems Department (LSD) of ELI-NP facility in 2017. This laser system was intended to perform experiments within the research projects of LSD, as well as to the training of the young ELI-NP researchers on Ti:sapphire chirped pulse amplification and femtosecond laser pulses characterization.

We describe in this paper the upgrading of the Avesta system in order to increase its peak power with more than one order of magnitude, from sub-TW levels to multi-TW levels. This increased output power is required for developments of ultrashort pulse metrology instrumentation and for applied research projects in preparation of the experiments at the ELI-NP facility. Section 2 of the paper describes the configuration of the sub-TW femtosecond commercial laser Avesta and measurement techniques for its femtosecond pulses characterization. In Section 3 a four-pass Ti:sapphire amplifier is presented, which has been designed to increase the chirped pulse energy with more than one order of magnitude. Section 4 presents the design of a vacuum temporal compressor for the multi-TW upgraded laser system. In Section 5, some proposed research projects based on the upgraded laser system are shortly described.

2. LOW ENERGY SYSTEM OVERVIEW

2.1. LASER SYSTEM DESCRIPTION

The table map of the Avesta laser is shown in Fig. 1. The femtosecond oscillator is based on Kerr-lens self-mode-locking. A pair of glass prisms, which gives rise to a

negative phase dispersion, are used in the optical resonator to compensate for the positive phase dispersion induced during the propagation of broadband laser pulses through the Ti:sapphire laser crystal. Under the optimal alignment, when the Ti:sapphire crystal is pumped by a frequency doubled CW Nd:YAG laser at 2.85 W, the laser oscillator is able to generate ultrashort pulses with ~4 nJ pulse energy, 90 MHz repetition rate, ~50 nm spectral bandwidth, corresponding to less than 20 fs pulse duration.

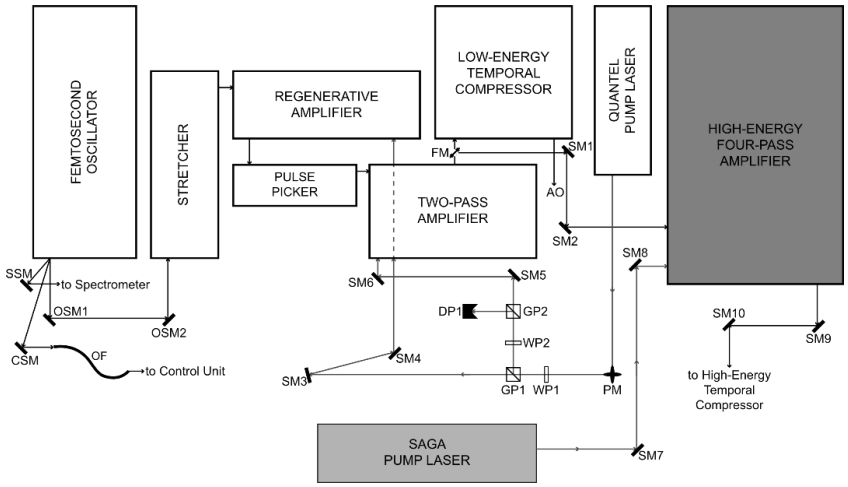

Fig. 1. Avesta laser system layout. SM1, SM2, SSM, CSM, OSM1, OSM2 – steering mirrors, HR broad-band with 800 nm central wavelength; SM3-SM6 – steering mirrors, HR@532 nm; GP1, GP2 – high-energy cube polarizers; WP1, WP2 – λ/2 waveplates at 532 nm; DP1 – beam dump; FM - flipping mirror, broad-band HR@800 nm; OF- optical fiber; SM9, SM10 – 50 mm diameter steering mirrors, HR broadband @800 nm; PM - periscope; AO – Avesta amplified femtosecond laser pulse. Grey colored modules belong to the Avesta upgraded configuration.

The main output beam of the femtosecond oscillator is steered into the temporal stretcher with two high reflectivity, large bandwidth dielectric mirrors, OSM1,2. Two additional weak beams, resulted from the wedged substrate of the oscillator's output coupler, are emitted along with the main output beam. One additional beam is directed through an optical fiber to the Control Unit of the Avesta system, which generates all synchronization electric pulses for Regenerative Amplifier (RA) and Pulse-Picker (PP) Pockels cells, pump laser flash-lamps triggering, and optical resonator Q-switching. The other beam is used to measure the femtosecond pulses spectrum with a spectrometer.

Oscillator femtosecond pulses are stretched with a ratio of ~6 ps/nm in a stretcher based on a M×1 magnification folded telescope configuration with a concave dielectric mirror and a single diffraction grating. For the femtosecond oscillator protection, a Faraday optical isolator is installed before the input of stretched laser pulses in the Regenerative Amplifier.

The RA schematic configuration is shown in Fig. 2a. Stretched broad-band pulses with a vertical linear polarization are injected into the RA through the RP1 dielectric film polarizer. The linear optical resonator is formed by two concave end mirrors RM3, RM4 of 1200 mm radius of curvature, two folding plane mirrors RM1, RM2, and two thin film polarizers RP1, RP2 tilted at 78.5^0 angle of incidence. The Ti:sapphire crystal, RTiSa, of 20 mm length in the normal direction, is tilted at Brewster angle. The RA path length is about 1.4 m, with a round-trip time of ~9.3 ns. A photodiode, RPD, is installed behind the RM4 mirror to observe the build-up of the RA train of pulses. A switchable RW$\lambda/4$ quarter-wave plate, rotated with a small-angle versus vertical polarization direction, is used to extract the laser energy from the RA resonator in the free-running operation, without seed laser pulses injection. The pump laser radiation is focused with the PL1 lens on the Ti:sapphire crystal to get ~0.95 mm pump beam diameter. The pump laser energy for RA and Two-pass Amplifier (TPA) is delivered by a 532 nm nanosecond Q-smart Quantel-laser, 220 mJ pulse energy, at 10 Hz repetition rate. The pump pulses of Quantel laser are split and attenuated through an external set-up containing steering mirrors, $\lambda/2$ wave-plates, and a beam dump (Fig. 1).

The vertically linearly polarized nJ-level seed pulses are injected in the optical resonator through a thin film polarizer RP1. If the PC1 Pockels cell is not activated, the injected laser pulse, after a trip RP1→RM1→RTiSa→RM2→PC1→RM3→ PC1→RM2→RTiSa→RM1→RP1, leaves the resonator and is rejected by the Faraday isolator in its way back towards stretcher. If a $V_{\lambda/4}$ voltage is applied on the PC1, the laser pulse will leave the resonator after the trip RP1→RM1 →RTiSa →RM2 →PC1→RM3→PC1→RM2→RTiSa→RM1→RP1→RP2→PC2→RM4→PC2→RP2 →RP1→RM1→RTiSa→RM2→PC1→RM3→PC1→RM2→RTiSa→RM1→RP1, because its linear polarization turns back to the vertical direction after last two passes through PC1. If the $V_{\lambda/4}$ voltage is applied before the first pass through the PC1 and is turned off before the second pass through it, the seed laser pulse remains horizontally polarized and stays inside the resonator until its suitable amplification. Fig. 2b shows a simulated regenerative train of pulses, amplified inside the RA resonator without extraction, for different pump-pulse energies.

After a number of round-trips, when the laser pulse energy reaches its optimum value, a short bell-shaped $V_{\lambda/4}$ voltage is applied to the PC2 Pockels cell. The laser pulse polarization changes from horizontal to vertical after two passes through PC2. An amplified chirped pulse of ~3.5 mJ energy, at 10 Hz repetition rate, leaves the resonator through the RP2 polarizer. Fig. 2c shows an oscilloscope screen with cavity dumping, where the last pulse of train has been extracted after a double pass through the activated PC2 Pockels cell.

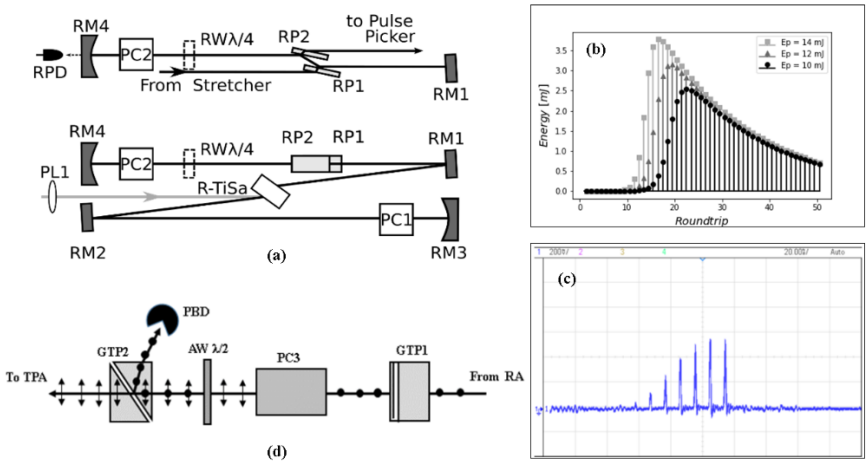

Fig. 2 – Regenerative Amplifier (RA) and Pulse-Picker (PP). (a) Schematic drawing of the Regenerative Amplifier. R-TiSa – Ti:sapphire crystal; RM1, RM2 – plane mirrors and RM3, RM4 - spherical concave mirrors, HR broadband dielectric with 800 nm central wavelength; PC1, PC2 - KDP Pockels cells; RP1, RP2 – thin film polarizers; Rλ/4 – quarter wave-plate at 800 nm wavelength; RPD –photodiode. PL1 – focusing lens, 350 mm focal length. (b) Calculated pulse amplification; pulse energy has been calculated using Frantz-Nodvik equation [12] (see details in Section 3), under assumption of flat top 532 nm pump spatial profile, uniform IR input beam spatial profile, 0.97 mm pump beam diameter in air in front of the Ti:sapphire crystal, 92% pump energy absorption in the RTiSa crystal, 5% round-trip losses in the optical resonator, 1 nJ seed pulse energy. (c) Oscilloscope screen with cavity dumping, the last pulse of the train has been extracted. (d) . Pulse-Picker schematic drawing. GTP1, GTP2 – Glan-Taylor polarizers; PC3 – Pockels cell; AWλ/2 – achromatic half-wavelength plate; PBD – beam dump.

A pulse-picker (PP), Fig. 2d, which consists of two crossed Glan-Taylor prism polarizers GTP1 and GTP2, and a PC3 Pockels cell is used to improve the nanosecond pulses energy contrast. We inserted an achromatic half-wavelength plate, AWλ/2, for the

control of the laser pulses linear polarization direction. When the AWλ/2 axis is parallel with the horizontal polarization direction of GTP2, without any voltage on PC3, vertically polarized laser pulses are reflected towards the beam dump PBD. To let the amplified laser pulses to go to the two-pass amplifier, a bell-shaped electric pulse $V_{\lambda/2}$ voltage of less than 7 ns pulse duration is applied to PC3. Without any voltage on PC3, if the AWλ/2 is adjusted to rotate the vertical beam polarization to horizontal polarization, laser pulses are transmitted through the GTP2 polarizer. This way, the free-running pulses extracted from RA resonator can be used for further alignment of the laser system. By tuning the AWλ/2 axis position, the output pulse energy from the laser system can be adjusted depending on the required beam parameters for experiments.

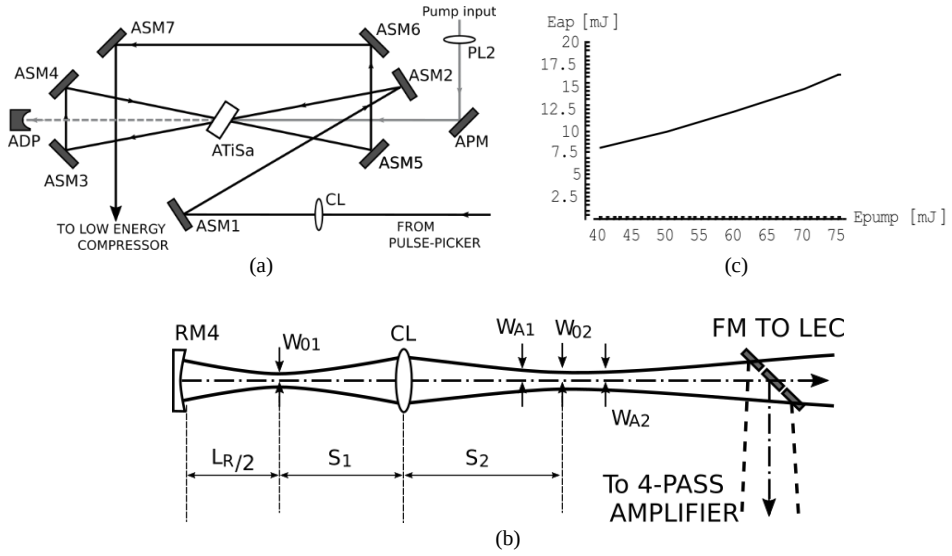

Fig. 3. Two-pass amplifier. (a) Schematic drawing. ATiSa –Ti:sapphire crystal; ASM1-ASM7 – steering mirrors, broadband HR@800 nm; CL – collimating lens; PL2 – pump beam focusing lens; APM - steering mirror, HR@532 nm (b) Infrared beam propagation through Avesta system. W_{01} – waist of the RA output beam; L_R – RA resonator optical length; Cl, collimating lens; FM, flipping mirror; S_1 distance of the collimated lens relative to the beam waist; S_2 – position the new quasi-Gaussian beam waist; W_{02} – waist of the collimated beam; $W_{A1} \approx W_{A2}$ beam radius in air in front of ATiSa crystal for both passes. (c) Calculated amplified pulse energy, $E_{ap,}$ versus pump pulse energy, E_{pump}, for 3.1 mJ input pulse energy.

The two-pass amplifier (TPA) is based on a Ti:sapphire crystal, ATiSa, with 8.14 mm × 6.14 mm input face and 8.35 mm thickness, tilted at Brewster angle (Fig. 3a).

The horizontally polarized beam is guided by the steering mirrors ASM1-ASM7 through the Ti:sapphire crystal and further towards the low-energy temporal compressor of the Avesta system. The position of the pump focusing lens, PL2, f = 600 mm focal length, is adjusted to get a pump beam diameter of ~1.7 mm in air in front of the Ti:sapphire crystal. The position of the CL collimating lens, f = 1000 mm focal length, is determined by the distance from the RM4 mirror to the ATiSa crystal.

The propagation of the RA quasi-Gaussian output beam through the Avesta system is shown in Fig. 3b. We consider a quasi-Gaussian beam with $M^2 = 1.3$ beam propagation factor. The W_{01} waist of the extracted beam from RA is given by $w_{01}= 0.39$ mm beam radius of the Gaussian beam multiplied by M. This waist is located at a distance of about 692 mm from RM4, corresponding to the AR resonator half-length, $L_R/2$. When the CL is positioned at a distance S_1 of about 1140 mm from the beam waist, it creates a new quasi-Gaussian beam with its waist located at $S_2 = 1380$ mm, practically in the middle of the distance between the two passes through the ATiSa crystal. The new beam waist radius will be ~0.73 mm and the estimated beam diameter in the front of Ti:sapphire crystal for both passes is 2×0.75 mm = 1.5 mm. Under these conditions, we calculated the amplified pulse energy versus pump energy pulse using Frantz-Nodvik equation [12], Fig. 3c.

The calculated beam diameter in front of the beam expander from the Low-Energy Temporal Compressor (LEC), located at about 2325 mm distance from the W_{02} waist in the actual system configuration, is 2.6 mm. After the 3 times beam expansion before temporal compression, it results an output beam diameter of ~7.8 mm.

2.2. CHARACTERIZATION OF LASER SYSTEM PULSES

The laser oscillator measurements were performed at an average power of 270 mW and a pulse repetition rate of 90 MHz. A single-shot second-order auto-correlator, based on recording the spatial profile of non-collinear phase-matched second harmonic generated in a thin KDP crystal, has been used for measuring the femtosecond pulse duration. The measured autocorrelation curve has FWHM of 32 fs, corresponding to pulse duration of 23 fs assuming Gaussian pulse shape (Fig. 4a). The measured optical spectrum is centered at 800 nm and has a bandwidth of 45 nm at FWHM (Fig. 4b). The calculated time-bandwidth product is 0.5, corresponding to 1.1 times the Fourier limit.

The output pulse energy from the regenerative amplifier is 3.4 mJ at pump energy of 10 mJ. The 2-pass amplifier delivers an output pulse energy of 15.2 mJ at a pump

energy of 82 mJ. After the compressor the CPA laser output pulses have the energy of 9.4 mJ, an energy stability of 2% RMS and a repetition rate of 10 Hz. The measured autocorrelation curve has the FWHM of 76 fs, corresponding to a pulse duration of 53 fs assuming Gaussian pulse shape (Fig. 5a). The central wavelength is 800 nm (Fig. 5b). The spectral bandwidth is 29 nm at FWHM (Fig. 5b). The calculated time-bandwidth product is 0.75, corresponding to 1.6 times the Fourier limit.

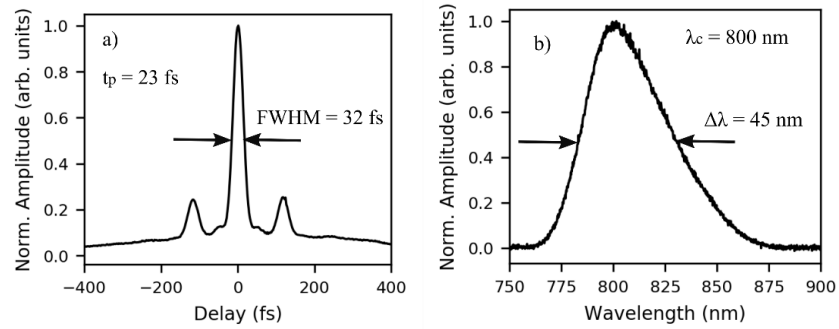

Fig. 4 – Autocorrelation curve (a) and optical spectrum (b) of the femtosecond oscillator.

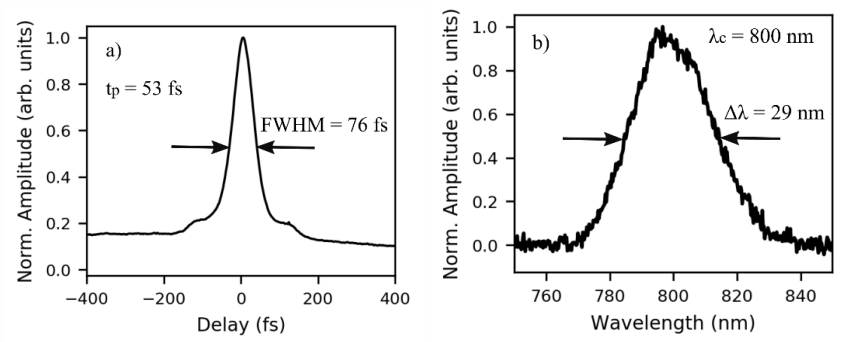

Fig. 5 – Autocorrelation curve (a) and optical spectrum (b) of the CPA laser system.

The nanosecond temporal contrast is 5×10^{-8}, measured using a fast photodiode and an oscilloscope. The value represents the ratio between the intensity of the highest pre-pulse existent within a few nanoseconds before the main pulse and the intensity of the main pulse. The picosecond temporal contrast has been measured with the 3rd order autocorrelator Tundra+ from Ultrafast Innovations. The contrast at 250 ps before the main pulse is 1.7×10^{-7} (see Fig. 6), while the pedestal at 10 ps corresponds to a contrast

of 10^{-4}.

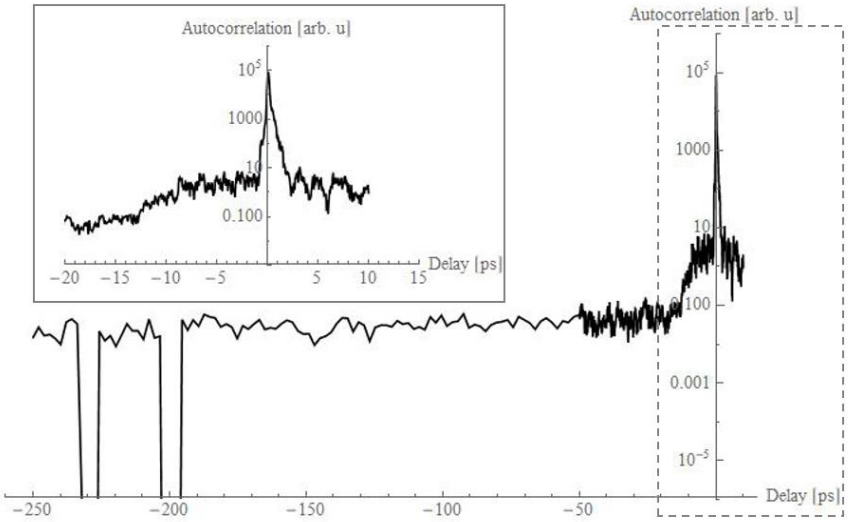

Fig. 6 – Picosecond temporal contrast of the CPA laser system, measured with the 3rd order autocorrelator. The range from -250 ps to -50 ps has been scanned with lower resolution. The sudden dropping of the autocorrelation value around -225 ps and -200 ps occurs due to alternately blocking each of the autocorrelator arms, in order to check the dynamic range of the device (approximately 12 orders of magnitude). The delay region around 0 that is marked with the dashed rectangle is zoomed in the left rectangle, for better resolving the pedestal.

3. HIGH ENERGY FOUR-PASS AMPLIFIER DESIGN

The four-pass amplifier (FPA) (Fig. 7) has been designed to amplify 10 Hz repetition rate output pulses from two-pass Avesta amplifier up to 250 mJ energy.

A flipping mirror has been installed between Avesta TPA and LEC (see Fig. 1). It sends the TPA output laser pulse alternatively towards LEC or TFP. Two steering mirrors, SM1 and SM2, guides the TPA laser pulse to the FPA input. Before amplification, the spatial profile of the laser pulse is 3 times expanded in a beam expander which consists in the plano-concave LE1C divergent lens with f_{1C} = -100 mm focal length and LE1X plano-convex convergent lens with f_{1X} = 300 mm focal length. The calculated input beam diameter in the designed system configuration is 3.6 mm,

corresponding to the 3700 mm propagation distance between the W_{02} waist of the infrared beam and the beam expander input. A small part of the laser beam energy is collected by an uncoated glass wedge, WD1, to be used for the input pulse characteristics measurement. After spatial expansion, the beam diameter increases up to ~10.8 mm diameter (at $1/e^2$ from peak intensity). The horizontally linear-polarized infrared laser beam is guided through the amplifier by MR1-MR11 steering mirrors, with broadband high reflectance around the 800 nm central wavelength. Ti:sapphire crystal rod, 16 mm diameter and 20 mm length, is fixed in a water cooled mechanical mount, connected to a chiller which maintains the circulating water temperature at 22 ± 1^0C.

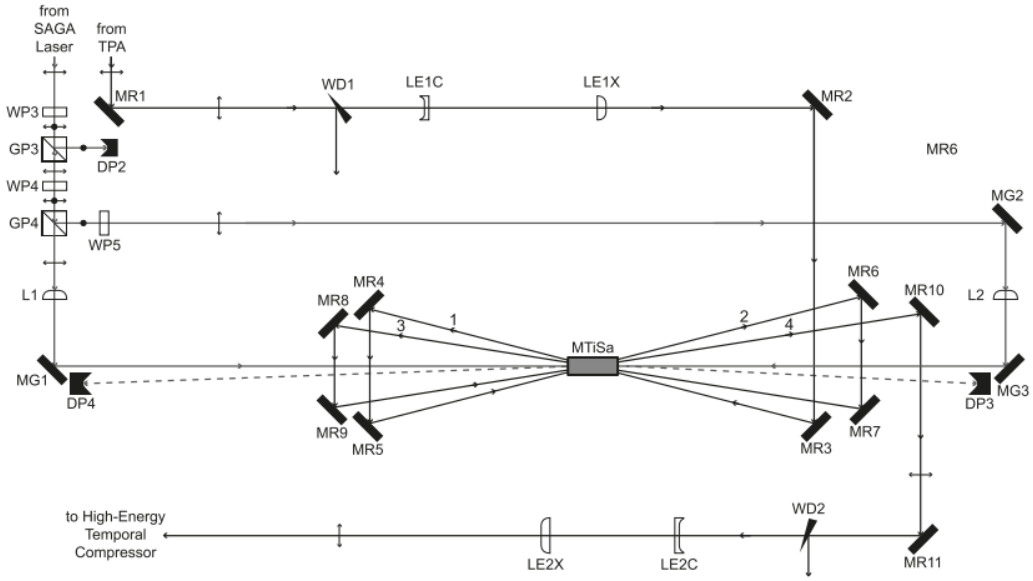

Fig. 7. Four-pass amplifier schematic drawing. MTiSa – Ti:sapphire crystal; MR1-11 – steering mirrors, broadband HR@800 nm; MG1-3 - steering mirrors, HR@532 nm; GP3-4 – high-energy cube polarizers; WP3-5 – λ/2 waveplates at 532 nm; LE1C, LE2C – plano-concave mirrors; LE1X, LE2X – plano-convex mirrors; L1-2 - focusing lenses; WD1-2 –glass wedges; DP3,4 – beam dump.

The pump nanosecond laser pulses generated by a SAGA HP (Thales Company) pump laser are 50-50% energy split to pump the MTiSa crystal through both end faces. The SAGA HP laser pulses, 1.8 J pulse energy at 532 nm wavelength, 10 Hz repetition rate, have a super-Gaussian, nearly flat-top, ~15 mm diameter spatial intensity beam

profile. The WP3-WP5 λ/2 waveplates and GP3, GP4 polarizing cubes are used to control the pump pulse energy and polarization. The MG1-MG3 steering mirrors, HR@532 nm, guide the pump beams to the MTiSa crystal end-faces. By using two 3000 mm focal length convergent lenses, L1 and L2, pump beams are slightly focused to get a pump beam diameter on MTiSa crystal end-faces of ~11.5 mm diameter. The remaining 532 nm radiation after Ti:sapphire crystal pumping is absorbed by DP3, DP4 dumps.

The amplified pulse energy, F_{amp}, for each pass through the MTiSa crystal was calculated using the Frantz-Nodvik equation [12-14]

$$F_{amp} = F_{sat} \ln\left\{1+\left[\exp\left(\frac{F_{in}}{F_{sat}}\right)-1\right]G_0\right\} \tag{1}$$

where $F_{sat} \approx 0.9$ J/cm^2 is the saturation fluence of Ti:sapphire crystal, F_{in} the input pulse fluence, and G_0 is the low signal exponential gain ($F_{in} << F_{sat}$).

$$G_0 = \exp\left[\frac{F_{lav}}{F_{sat}}\right], \quad F_{lav} = \eta_{qe} \times \eta_{qd} \times \eta_{abs} \times F_p \tag{2}$$

where F_{lav} is the available laser fluence for amplification, accumulated on the upper laser level in the crystal volume per unit surface of input face, F_p is the pump fluence accumulated trough both pumped faces, η_{qe} quantum efficiency (0.8 for Ti:sapphire), η_{qe}, quantum defect is the ratio between pump wavelength and laser wavelength, and η_{abs} is the pump energy absorption efficiency in the laser crystal. For iterative calculation

$$\begin{aligned} F_{lav}^{(i+1)} &= F_{lav}^{(i)} - (F_{out}^{(i)} - F_{in}^{(0)}) \\ F_{in}^{(i+1)} &= F_{out}^{(i)} \end{aligned} \tag{3}$$

The calculated output pulse energy, E_{out}, depending on 532 nm nanosecond pump pulse energy, E_p, for different E_{in} input pulse energy values, is shown in Fig. 8.

Amplified pulse energy can be controlled in the range of 80-220 mJ by changing both TPA and FPA pump energies in the limits of 62 mJ ± 15%, respectively 1200 mJ ± 15%. The range of output pulse energy variation can be increased by adjusting the seed pulse energy of TPA using AWλ/2 waveplate from the Pulse-Picker module. A small part of the output laser beam is collected by an uncoated glass wedge, WD2, to monitor

the amplified laser pulses. The output beam is 2× expanded up to ~22 mm beam diameter using an telescope consisting in a 25 mm diameter plano-concave spherical lens LE2C, f_{2C} = -100 mm focal length, and a 50 mm diameter plano-convex LE2X, f_{2X} = 200 mm focal length. Considering the maximum amplified laser pulse energy of 220 mJ and a beam diameter of ~22 mm diameter, the average fluence would be restricted to ~57 mJ/cm^2, which represents a safe value for the diffraction gratings from the High-Energy Temporal Compressor (HEC) of the upgraded laser system.

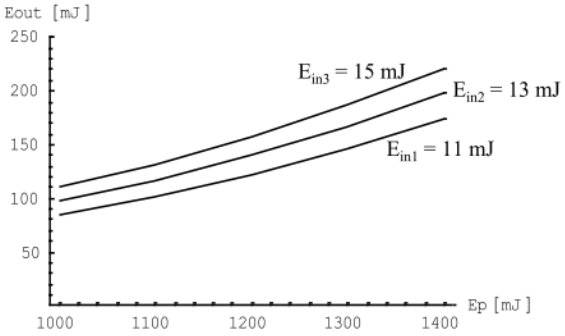

Fig. 8. FPA pulse energy.

The difference between the pump and the laser photon energy, termed as quantum defect, is the major source of Ti:sapphire crystal heating. In an end-pumped crystal rod, a temperature gradient is established as a result of pump heating and water cooling along the cylindrical surface, with the highest temperature in the center of the rod. The temperature-dependent variation of the refractive index constitutes the major contribution of the thermal lensing. Assuming an uniform internal heat generation by optical pumping, the focal length of the induced thermal lens is [15]

$$f_{TL} = \frac{2KA_p}{P_h \frac{dn}{dT}} \tag{4}$$

K is the Ti:sapphire thermal conductivity, $dn/dT = 6.1\times10^{-6}K^{-1}$ is the refractive index variation with temperature, $P_h = (1-\eta_{qd})\eta_{abs}P_p$ is the power dissipated as heat in the crystal, A_p is the heated cross-sectional pump area. For the highest average pump power P_p = 14 W, the calculated thermal lens is ~250 m. Because the thermal lens is much longer than the distance between passes through the crystal, the equivalent thermal lens

after 4 passes would be four times shorter, about 62 m. This slight focusing could be compensated by slightly defocusing the input beam expander from the collimation condition $f_{1C} + f_{1X} = L_1$, where L_1 if the distance between focal planes of the lenses. By decreasing this distance with δ = -1.5 mm, the induced divergence, corresponding to a lens with $f_{1e} \approx f_{1X}^2/\delta$ = -60 m, could compensate for the thermal lens effect.

4. HIGH-ENERGY TEMPORAL COMPRESSOR DESIGN

The parameters to be used as input for the High-Energy Temporal Compressor are 220 mJ and 22 mm beam diameter as generated by the high-energy 4 pass amplifier after the beam expander telescope, corresponding to an estimated fluence of 0.057 J/cm^2. The spectral bandwidth at the input of the compressor is smaller than the 29 nm FWHM bandwidth at the entrance in the high-energy 4-pass amplifier, due to gain driven spectral narrowing. Consequently, a suitable value of 30 nm FWHM of spectral bandwidth was used as input for the design of the compressor. The compressor shall simultaneously fulfill at least the conditions analyzed in the following sections.

4.1. Dispersion compensation

The compressor shall compensate the dispersion from the stretcher and from the materials used along the amplification chain. The accumulated spectral phase along the amplification chain calculated for the optical stretcher and materials is presented in Table 1. The stretcher dispersion calculation corresponds to the measured value of 245 ps pulse duration at the exit of the stretcher for the 40 nm bandwidth of the oscillator pulse. A streak camera was used for the pulse duration measurement of the 44 nm full width at half maximum (FWHM) stretched pulse in order to confirm the stretching factor of 5.94 ps/nm [16].

An input pulse with Gaussian spectrum and Fourier transform limited (FTL) FWHM duration of 31.4 fs was considered, corresponding to 30 nm of bandwidth FWHM at 800 nm central wavelength. Best compression of 33 fs pulse duration, was obtained with the residual spectral phase shown in Fig. 9, with dispersion compensation between GDD and TOD.

Several groove densities were considered, in the range 1200 lines/mm to 1780 lines/mm [17]. For 1200 lines/mm the angle separation between the diffracted beam and

the incident beam is too small, so there is a geometrical conflict between the grating and roof mirror while for 1780 lines/mm the separation angle is too big. The optimal grove density was selected to be 1480 lines/mm.

Table 1

Accumulated spectral phase of 2nd order (group delay dispersion – GDD), 3rd order (Third order dispersion – TOD) and 4th order (fourth order dispersion - FOD) in stretcher, materials, and compressor.

Sub-system		GDD (fs^2)	TOD (fs^3)	FOD (fs^4)
Stretcher	angle: 25.65 (deg)	1.99E+06	-4.31E+06	1.44E+07
	distance: 550.00 (mm)			
Materials before upgrade		9.55E+04	6.85E+04	-2.57E+04
Materials after upgrade		1.01E+05	7.27E+04	-2.72E+4
Compressor	angle: 52.21 (deg)	-2.09E+06	4.37E+06	-1.38E+07
	distance: 426.30 (mm)			
Total		-339.72	845.60	5.18E+5

.

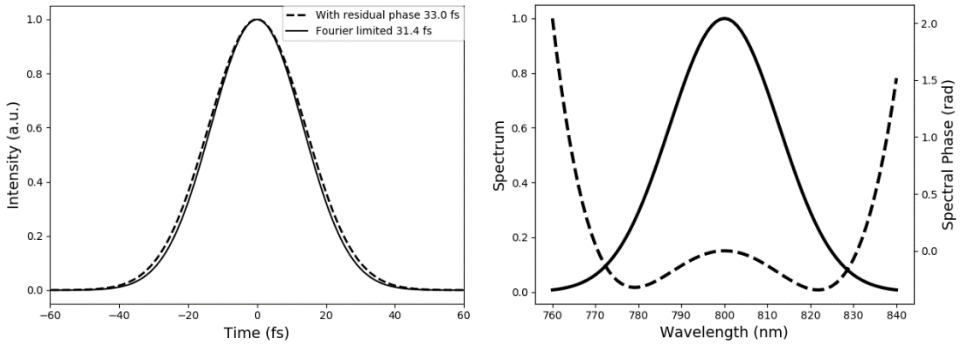

Fig. 9. Left: Compressed pulse after upgrade and Right: Spectrum (continuous line) and spectral phase (dashed line) of the compressed pulse after upgrade

4.2. Vacuum compatibility

The compression shall take place in vacuum, in order to avoid subsequent accumulation of non-linear phase (B-integral) when operated in air at high fluence. As a consequence, the compressor shall be compact for reducing the cost of vacuum

chamber and pumping system. The general design for a compressor uses 4 gratings or folded versions that use two gratings and a roof mirror or one grating and two roof mirrors. The adequate design in this case is using two gratings as depicted in Fig. 10, in order to avoid geometrical conflicts.

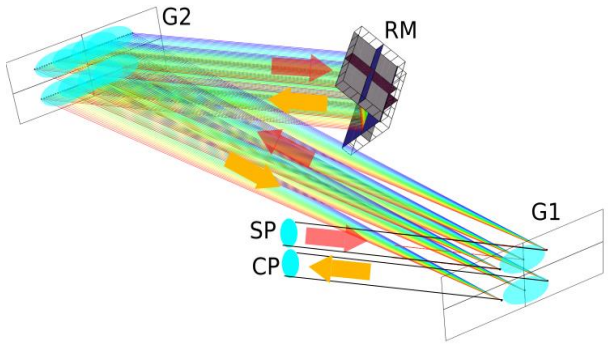

Fig. 10: Ray tracing for the two gratings and one roof mirror design of the compressor. SP is the stretched pulse, G1 is the first grating, G2 is the second grating, RM is the roof mirror that folds the compressor and sends the beam in a lower plane, CP is the compressed pulse. The arrows indicate the beam propagation direction.

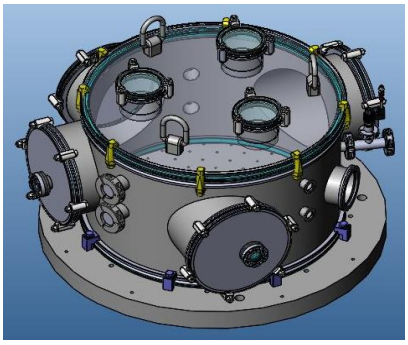

Fig. 11. Vacuum chamber with ports

The vacuum chamber designed to host the compressor is depicted in Fig. 11. The large flanges are following the standard ISO-K 250 for interface compatibility with the ELI-NP high power laser system (HPLS) beam lines of 100 TW and 1 PW. It shall be

used also for testing optical beam dump for the HPLS beams. The inner diameter of the chamber is 600 mm. The targeted residual pressure in the compressor is 10^{-5} mbar.

The input and output ports for the compressor are CF 2.75" vacuum flanges with 4 mm thick fused silica, 38 mm diameter clear aperture, broadband anti-reflection coated. These flanges are connected at different heights on the ISO-K 250 flanges. The three ports on top provide the possibility to visualize the gratings of the compressors through viewports.

4.3. Temporal contrast preservation

In order to avoid deterioration of the temporal contrast of the output pulse, the spectral bandwidth of the input pulse shall be preserved at the exit of the compressor. This is accomplished using large enough gratings that catch all the rays from the input beam. The general rule to avoid significant spectral hard clip is to use a bandwidth three times larger than the FWHM bandwidth of the pulse at the entrance in the compressor. Thus, the chosen gratings sizes are 70 mm height and 50 mm width for the first grating and 70 mm height and 140 mm width for the second grating.

4.4. Damage threshold

The compressor shall resist at the fluence of the input pulses as mentioned above, taking into account the possible hot spots in the near field beam profile of the input pulses and the technological limits in the grating fabrication. The damage threshold of diffractive gratings can reach up to 0.2 J/cm^2 for gold gratings and p-polarized light. Nevertheless, the operation fluence of such gratings is limited to 0.05-0.1 J/cm^2 in order to avoid damage from beam profile inhomogeneity also known as hot spots. The conservative approach here is to stay a factor of three below the damage threshold of the diffractive gratings, condition fulfilled in the presented design.

4.5. High efficiency and stability

The compressor shall have reduced losses and shall be stable. The overall efficiency of the compressor can be estimated as being the power fourth of the diffraction efficiency for the diffraction grating used. This is why a master grating with typical efficiency larger than 90% has to be considered in general for the compressors instead

of a replica grating with 86% efficiency. These values correspond to 65% and 54% compressor transmission, respectively.

Also, the substrate shall have reduced expansion coefficient in order to avoid thermal fluctuations of the compression factor through the thermal variation of the groove density. Zerodur and fused silica are good options for the material substrate while the borosilicate glass shall be avoided, as the thermal expansion coefficient is roughly one order of magnitude higher than for the fused silica and zerodur [18].

5. PROSPECTS ON RESEARCH

The laser system described here will serve two main purposes, training of the next generation of specialists in ultra-intense lasers and extreme light related research. The research part includes developments of instrumentation for metrology of the ultrashort pulses but also pure and applied research in preparation of the experiments at the ELI-NP facility. Several examples of on-going research will be described here further.

5.1. Spectral broadening for post-compression

One complementary method to generate shorter pulses is related to spectral broadening through non-linear self-phase modulation and post-compression of ultrashort pulses, down to single cycle electromagnetic wave fields. A technique scalable to TW, and PW peak powers was initially demonstrated in [19], using thin transparent materials. Recent efforts, reported in [20-22], target to demonstrate the feasibility of such technique for TW- and PW-class pulses in order to boost the available peak power at ELI-NP in the 20 PW per arm and above. Various thin films of transparent materials are used in vacuum to obtain the spectral broadening. Characterization of the optical non-linearities for various materials is mandatory and can be performed at the facility reported here, taking advantage of the centimeter-sized beams that will be available with high fluence. Standard methods to characterize the third order non-linearities of transparent materials, such as Z-scan and I-scan are already implemented at Avesta system. The results can be of use in the broader non-linear optics context of localized optical wave structures [23,24].

Post-compression quality of the broadened pulse will be realized using at least one of the two compressors developed in house. One of them is a chirped mirror compressor while the other is a single prism compressor [25] suitable for smaller aperture beams but with higher compression ratio capability.

5.2. Laser-induced damage threshold measurements

Not only the non-linear effects, but also the damage threshold of the optical components is critical for proper implementation of experiments referred above. The in-house capability of qualification for laser induced damage threshold of optical components is also essential in the operation and maintenance for HPLS. It will allow reliable operation and reduced down-time for HPLS as well as development of optics coatings for the envisaged experiments at ELI-NP.

Qualification of the optical coatings and materials will be performed on large aperture beams, having diameters in the range of few millimeter and above. The international standards for measurement of laser induced damage threshold recommends for femtosecond pulses the use of laser spot size on target larger than 200 μm (see Note 1 of Subsection 6.2.3 of [26]). In practice it was observed that the reported damage threshold fluence is actually smaller when large laser beam diameters are used [27,28], due to averaging on a larger number of micrometer sized defects of the optic, and, therefore, using a too small spot size gives unrealistically high, too optimistic values of the damage threshold.

5.3. Synchronization and coherent combination of ultrashort pulses

The most promising technology for up-scaling towards 100 PW class lasers is the coherent combination of ultrashort pulses. ELI-NP can preserve the status of the most powerful laser worldwide if coherent combination of the two arms with nominal 10 PW peak power is achieved through synchronization and phasing, in a field corresponding to 20 PW using collinear [29] or non-collinear [30,31] approach.

In prospective experiments at Avesta system, the beams from the two arms will be amplified in parallel amplifiers and the focal spot position jitter and temporal overlap will be qualified using various methods that include the near field and far field monitoring, and interferometric measurements of the optical path difference fluctuations [32].

6. CONCLUSIONS AND OUTLOOK

Based on a commercial sub-TW Ti:sapphire femtosecond laser amplifier, we designed an upgraded multi-TW femtosecond laser system. Using an additional four-

pass Ti:sapphire amplifier, the energy of the commercial laser output chirped pulses can be increased from 15 mJ up to 220 mJ, with a 22 mm diameter and 0.057 J/cm^2 average fluence, at 10 Hz repetition rate. A two-diffraction gratings vacuum temporal compressor was designed to compensate for phase dispersion in stretcher and materials of amplifier stages. For an ideal input laser pulse with Gaussian spectrum and 31.4 fs Fourier transform-limited (FTL) FWHM duration, we calculated a best compression output pulse of 33 fs duration, 1.05 times FTL. Considering a 65% compressor transmission, multi-TW laser pulses would be generated by the upgraded femtosecond laser system.

Using this multi-TW laser system, extreme light related research will be developed, such as spectral broadening for post-compression, laser induced damage threshold in femtosecond laser field, synchronization and coherent combination of ultrashort laser pulses.

Acknowledgements. This work was realized through "Nucleu" program, funded by the Romanian Ministry for Education and Research, project number 19 06 01 05 2020. Work has been supported by the Extreme Light Infrastructure Nuclear Physics (ELI-NP) Phase II, a project co-financed by the Romanian Government and the European Union through the European Regional Development Fund and the Competitiveness Operational Programme (1/07.07.2016, COP, ID 1334). Authors acknowledge the constructive comments from G. Nemes during the preparation of the manuscript.

REFERENCES

1. D. Strickland, G. Mourou, *Optics Communications*, **56**, 219–221 (1985).
2. S. Backus, C.G. Durfee III, M.M. Murnane, H.C. Kapteyn, *Rev, Sci. Instrum.,* **69**, 1207-1223 (1998).
3. V. Yanovsky, V. Chvykov, G. Kalinchenko, P. Rousseau, T. Planchon, T. Matsouka, A. Maksimchuk, J. Ness, G. Cheriaux, G. Mourou, K. Krushelnick, *Optics Express*, **16**, 2109-2114 (2008).
4. M. P. Kalachnikov, V. Karpov, H. Schonnagel, W. Sandner, L*aser Physics***, 12**, 368–374 (2002).
5. J. H. Sung, S.K. Lee, T.J. Yu, T.M. Jeong, J.Lee, Opt. Lett., **35**, 3021 (2010).
6. H. Kiriyama, M. Mori, Y. Nakai, T. Shimomura, H. Sasao, M. Tanoue, S. Kanazawa, D. Wakai, E. Sasao, H. Okada, I. Daito, M. Suzuki, S. Kondo, K. Kondo, A. Sugiyama, P.R. Bolton, A. Yokoyama, H. Daido, S. Kawanishi, T. Kimura, T. Tajima, *Opt. Lett*., **35**, 1497 (2010).
7. J.H. Sung, H.W. Lee, J.Y. Yoo, J.W. Yoon, C.W. Lee, J.M. Yang, Y.J. Son, Y.H. Jang, S.K. Lee, C.H. Nam, *Opt. Lett*., **42**, 2058 (2017).
8. W. Li, Z. Gan, L. Yu, C. Wang, Y. Liu, Z. Guo, L. Xu, M. Xu, Y. Hang, Y. Xu, J. Wang, P. Huang, H. Cao, B. Yao, X. Zhang, L. Chen, Y. Tang, S. Li, X. Liu, S. Li, M. He, D. Yin, X. Liang, Y. Leng, R. Li, Z. Xu, *Opt. Lett*., **43**, 5681 (2018).

9. G. A. Mourou, T. Tajima, S.V. Bulanov, *Rev. Mod. Phys.*, **78**, 309-371 (2006).
10. M.A.M. Hafz, T.M. Jeong, I.W. Choi, S.K. Lee, K.H. Pae, V.V. Kulagin, J.H. Sung, T.J. Yu, K.H. Hong, T. Hosokai, J.R. Cary, D.K. Ko, J. Lee, *Nat. Photon.*, **2**, 571 (2008).
11. D. Ursescu, G. Cheriaux, P. Audebert, M. Kalashnikov, T. Toncian, M. Cerchez, M. Kaluza, G. Paulus, G. Priebe, R. Dabu, M.O. Cernaianu, M. Dinescu, T. Asavei, I. Dancus, L. Neagu, A. Boianu, C. Hooker, C. Barty, C. Haefner, *Romanian Reports in Physics*, **68**, S11-S36 (2016).
12. L.M. Frantz, J.S. Nodvik, *Journal of Applied Physics*, **34**, 2346-2349 (1963).
13. W. Koechner, *"Solid State Laser Engineering*", Springer Science+Business Media, New York, USA, 2006, pp. 156-171.
14. R. Dabu, *"Lumina Extrema – Lasere de mare putere",* Editura Academiei Romane, Bucuresti, 2015, pp. 21-24, 63-74.
15. W. Koechner, *"Solid State Laser Engineering*", Springer Science+Business Media, New York, USA, 2006, pp. 423-457.
16. M. Masruri, R. Secareanu, R. Fabbri, D. G. Matei, D. Ursescu, *"Temporal characterization of shaped picosecond pulses using a streak camera"* in *"ELI-NP internal report 2018",* vol. 1 (2018), available on request.
17. Jeff Squier, Chris P. J. Barty, François Salin, Catherine Le Blanc, and Steve Kane *Applied Optics*, **27** (9) 1638 (1998).
18. J.H. Burge, T. Peper, and S.F. Jacobs, *Applied Optics* **38**, 7161-7162 (1999).
19. C. Rolland and P.B. Corkum, *J. Opt. Soc. Am. B* **5** (3), 641 (1988.)
20. S.Yu. Mironov, J. Wheeler, R. Gonin, G. Cojocaru, R. Ungureanu, R. Banici, M. Serbanescu, R. Dabu, G. Mourou, E.A. Khazanov, *Quantum Electronics* **47** (3) 173–178 (2017).
21. Philippe Lassonde, Sergey Mironov, Sylvain Fourmaux, Stéphane Payeur, Efim Khazanov, Alexander Sergeev, Jean-Claude Kieffer, Gerard Mourou *Laser Phys. Lett.* **13** 075401 (2016).
22. D. M. Farinella, J. Wheeler, A. E. Hussein, J. Nees, M. Stanfield, N. Beier, Y. Ma, G. Cojocaru, R. Ungureanu, M. Pittman, J. Demailly, E. Baynard, R. Fabbri, M. Masruri, R. Secareanu, A. Naziru, R. Dabu, A. Maksimchuk, K. Krushelnick, D. Ros, G. Mourou, T. Tajima, and F. Dollar, *J. Opt. Soc. Am. B* **36**, A28-A32 (2019).
23. D. Mihalache, *Romanian Reports in Physics* **67**, 1383 (2015).
24. D. Mihalache, *Romanian Reports in Physics* **69**, 403 (2017).
25. Selcuk Akturk, Xun Gu, Mark Kimmel, and Rick Trebino, *Opt. Express* **14**, 10101 (2006).
26. ISO 21254-1:2011, Lasers and laser-related equipment - Test methods for laser radiation- induced damage threshold - Part 1: Definitions and general principles, ISO, Geneva, Switzerland.
27. L. Jensen, S. Schrameyer, M. Jupé, H. Blaschke, and D. Ristau, *Proc. SPIE 7504, Laser-Induced Damage in Optical Materials: 2009*, 75041E (2009).
28. Han Wei, Wang Fang, Zhou Li-Dan, Feng Bin, Jia Huai-Ting, Li Ke-Yu, Xiang Yong, Zheng Wan-Guo *Chinese Phys. B* **21**, 077901 (2012).
29. R Banici, D Ursescu, *EPL (Europhysics Letters)* **94** (4), 44002 (2011).
30. L Ionel, D. Ursescu, *Romanian Reports in Physics*, **63** (3), 500 (2010).
31. L Ionel, D. Ursescu, *Optics Express* **24** (7), 7046-7054 (2016).
32. S. Simion, C. Blanaru, D. Ursescu, *Romanian Journal of Physics*, **62**, 644 (2010).